Influence of phosphoric acid on the electrochemistry of lead electrodes in sulfuric acid electrolyte containing antimony

S. Venugopalan

Chemical Batteries Division, Power Systems Group, ISRO Satellite Centre, Bangalore-560017 (India)

Abstract

The influence of phosphoric acid (0 to 40 g l^{-1}) on the Pb/PbSO$_4$ reaction and the kinetics of hydrogen evolution on pure, smooth lead and lead alloy electrodes is studied via galvanostatic polarization in the linear and Tafel domains with and without antimony (0 to 10 mg l^{-1}) addition to the H$_2$SO$_4$ (3 to 10 M) electrolyte. Phosphoric acid is found to offset significantly the adverse effect of antimony. H$_3$PO$_4$ is also found to increase the hydrogen overpotential without affecting the Pb/PbSO$_4$ reaction. This implies that the open-circuit corrosion of lead and the consequent hydrogen evolution rate on lead are reduced in the presence of H$_3$PO$_4$. The beneficial effects of H$_3$PO$_4$ additive are found to be optimum at around 20 g l^{-1}. Suppression of hydrogen evolution on the negative electrode, a crucial criterion for sealed cell operation, can be achieved using a H$_3$PO$_4$ additive.

Introduction

In the area of secondary batteries, the lead/acid battery occupies a pre-eminent position as a long-life, low-cost source of power. The modern trend is to operate this battery in a sealed configuration. When used in sealed cells, conventional grid alloys for the positive electrodes induce antimony poisoning [1] of the negative electrodes. Eventually this results in cell failure through excessive hydrogen evolution. By contrast, antimony-free alloys provide only a short deep-discharge cycle life [2]. Hence, low antimonial lead alloys are recommended for sealed cells [3, 4]. Release of antimony even from the low-antimonial positive grid is, however, unavoidable.

One of the approaches to solving the problem of high hydrogen gassing through antimony poisoning is to have an additive in the electrolyte. Addition of phosphoric acid (H$_3$PO$_4$) or its salt, either to the electrolyte or to the positive active material, has been undertaken as a means for increasing cycle life, especially with non-antimonial positive grids. Although numerous reports [5–23] are available on the effect of H$_3$PO$_4$ on the electrochemistry of the PbO$_2$/PbSO$_4$ electrode, surprisingly, there are very few published data on its influence on the Pb/PbSO$_4$ electrode. With regard to the latter electrode, there are only brief studies in which it has been pointed out that H$_3$PO$_4$ additive has no effect either on the Pb/PbSO$_4$ electrode reaction [10, 15] or on the open-circuit passivation potential of Pb in H$_2$SO$_4$ [11]. It has also been reported in a recent publication [24] that H$_3$PO$_4$ increases the overpotential for the hydrogen-evolution reaction (HER) on lead–calcium alloys in H$_2$SO$_4$ electrolyte. Moreover, there

is no reference in the literature of any possible interaction of phosphoric acid and antimony that may influence the lead/acid battery negative electrode performance. The concentration of H_3PO_4 additive has to be re-optimized due to the use of higher than normal concentration of H_2SO_4 in sealed cells. The objective of the present investigation is to elucidate the effect of H_3PO_4 on the electrochemical processes on lead and lead alloy materials in the presence of antimony in sulfuric acid electrolyte.

Experimental

Pure lead (99.97 wt.%) and Pb–0.08 wt.% Ca–0.3 wt.% Sn alloy sheet grid materials obtained through the courtesy of UB–MEC Batteries Ltd., India, were used as test specimens. The composition of these alloys was determined using ICP–EDAX techniques (inductively coupled plasma spectroscopy–energy dispersive analysis of X-rays). The electrodes were mounted in a tight fitting Teflon holder to expose an area of 4 cm^2 to the electrolyte. The surfaces were prepared by polishing with successively finer grades of silicon carbide with distilled water as lubricant. The electrodes were examined under an optical microscope to ensure absence of deep scratches and embedded abrasive particles. The electrodes were degreased in trichloroethylene and etched for 10 s in an acetic acid/hydrogen peroxide mixture. They were then quickly rinsed with distilled water and introduced into the deoxygenated test solution. Each experiment was carried out with a newly polished electrode and with a fresh portion of the solution.

Polarization experiments on electrodes were carried out in a Pyrex cell (Fig. 1) assembly. This was fitted with ungreased, ground-glass joints to accommodate the test electrode, electrolyte bridges for the counter electrode, a Luggin bridge for the reference electrode, and the inlets for hydrogen purging, additives, a thermometer and a water seal for a rotating stirrer.

A large sheet of PbO_2 coated, pure lead served as the counter electrode. This was situated in a separate compartment and was connected to the test cell through electrolyte bridges that each had fritted glass discs at the tip to prevent direct access of evolved oxygen to the working electrode. This arrangement also prevented a build-up in the concentration of Pb^{2+} in the test electrolyte. The anode and cathode compartments of the cell were separated by solution-lubricated glass stopcocks in addition to the fritted glass discs.

All potentials are referred to a Hg/Hg_2SO_4 reference electrode in sulfuric acid of the same molarity as the test solution. This electrode was positioned adjacent to the centre (2 mm away) of the test electrode.

All chemicals were of analytical reagent (AR) grade and double-distilled water was used throughout. Test solutions of 3.67, 5.298, 6.008, 8.0432 and 10.09 M H_2SO_4 were prepared. AR grade H_3PO_4 was used as such. A stock solution of Sb(III) was prepared by dissolving AR grade antimony metal powder in hot H_2SO_4 (10 M). Antimony(III) stock solution was analysed both by potentiometric titration and by atomic absorption spectrometry (AAS) [25].

An Aplab power supply, in combination with a current regulator, was used for galvanostatic polarization. A Keithley model 195A DMM was used to monitor the current. The potential of the working electrode was measured using a Keithley 617 electrometer and a Datel DVC-8500 as a black-off supply. The response of the electrode potential as a function of current and time was recorded with a Philips PM 8134 x–y–t recorder. A Julabo F10-HC refrigerated circulator was used to maintain the temperature of the test cell at 25 ± 1 °C.
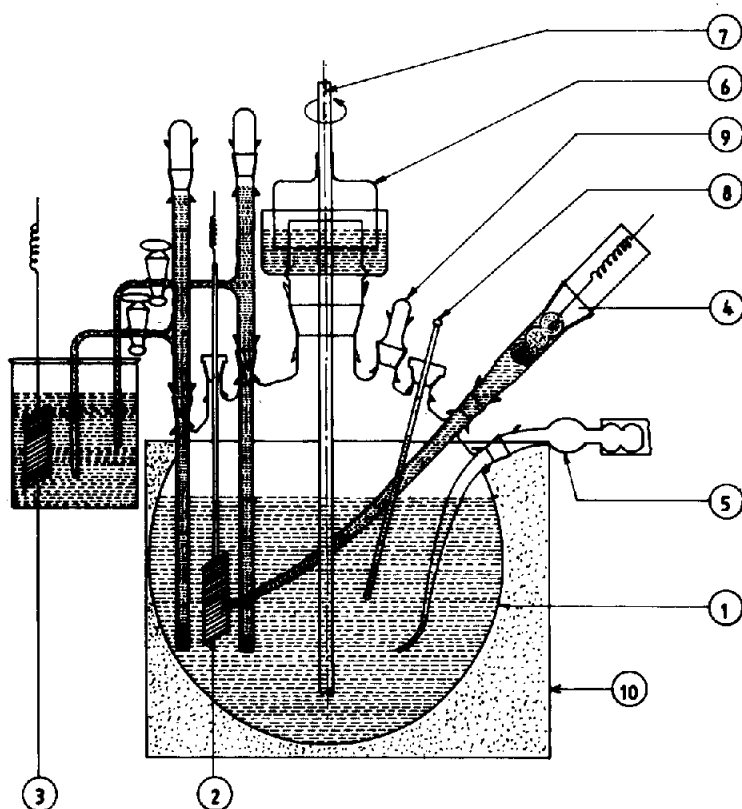
Fig. 1. Schematic view of electrochemical cell used for polarization studies: (1) round bottom flask (500 ml capacity); (2) working electrode (test specimen); (3) counter electrode; (4) reference electrode (Hg/Hg$_2$SO$_4$/H$_2$SO$_4$); (5) inlet for H$_2$ gas; (6) water seal; (7) rotating stirrer; (8) thermometer; (9) ground-glass joint for the introduction of additives, and (10) thermostat.

Procedure

Prior to measurements, the working solution was de-aerated in the cell with pure (IOLAR I grade) hydrogen for 1 h. The working electrode was then introduced and kept cathodically polarized (1 mA cm^{-2}) from the moment of insertion in the electrolyte to prevent its spontaneous corrosion from creating a build-up of Pb^{2+} in solution. The current was then increased to about 100 mA cm^{-2} (apparent area) and continued for 10 to 15 min. After this polarization treatment [26–28] at high current density, the electrode was in a stable condition and suitable for the measurement of hydrogen overpotential at various current densities. The polarization treatment probably removes dissolved Pb^{2+} (if any) in the vicinity of the test electrode so that distortion of the polarization curve for the HER is minimized [27]. This hydrogen-evolution treatment has also been found to smooth the surface [28]. The steady-state potential at the highest current density 100 mA cm^{-2} was recorded. The steady-state potentials at other current densities were recorded (2 min after setting a given current) by decreasing the current in steps. The steady-state potential for a given current density was independent (within ±1 mV) of the direction of the sweep, provided the current densities were in the range of 0.5 to 100 mA cm^{-2}. Subsequent to galvanostatic polarization, the

4

open-circuit potential was monitored with time to get the steady-state corrosion potential (E_{cor}). For studies with additives, 1 h of equilibration time in a well-stirred solution was applied prior to polarization measurements. In all experiments, the solution was kept stirred and hydrogen gas was bubbled through it.

Results and discussions

Tafel polarization curves for the HER obtained under various conditions are presented in Figs. 2–6.

Figure 2 shows the results obtained during steady-state, galvanostatic, cathodic polarization for smooth lead in hydrogen-saturated, well-stirred sulfuric acid solution that was initially free of lead ions (a), and in solution pre-saturated with lead sulfate ((b) and (c)).

It is well documented that the cathodic polarization of lead in sulfuric acid gives rise to a hysteresis curve. This was originally attributed to adsorption/desorption of SO_4^{2-} ions [29–32]. Recently, however, it has been established by an initial, intense, cathodic polarization of the test specimen that the hysteresis is mainly due to the cathodic discharge of dissolved lead ions present as an unintended impurity in the solution [27] and which, thereby, causes both an error in the current measurement and also a change in the morphology of the lead surface.

In the present work, it was considered desirable to verify the above mechanism independently and then ensure that the unavoidable presence of Pb^{2+} ions in solution will not vitiate the Tafel plot characteristics of the HER. The data of Fig. 2 clearly show the following features:
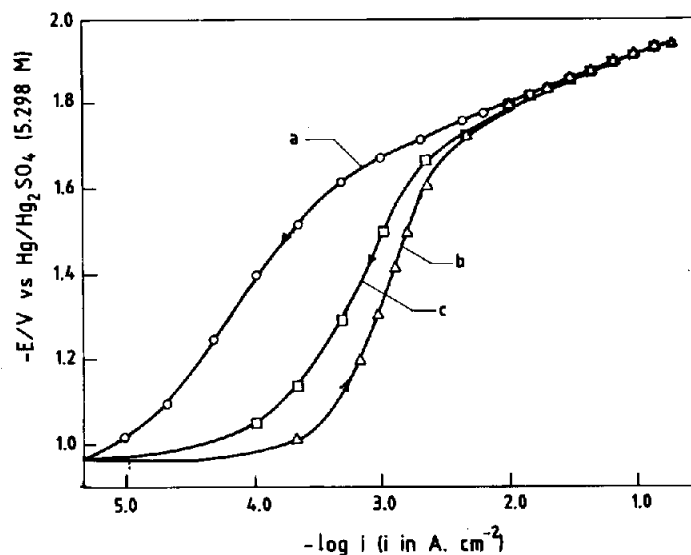

Fig. 2. Tafel plots for HER on smooth, sheet lead electrode in hydrogen saturated, well stirred, H_2SO_4 (5.298 M) solution at 25 ± 1 °C. Curve (a) reverse sweep in solution depleted of Pb^{2+} ions; curve (b) forward sweep in solution saturated with Pb^{2+} ions, and curve (c) reverse sweep in solution saturated with $PbSO_4$.

(i) The initial rise in the polarization curve is due mainly to the establishment of a limiting current for lead deposition from the solution. This will cause a hysteresis between the forward and reverse sweeps of the polarization. Such a finding is in agreement with published results [27].

(ii) The steady-state Tafel plot for the HER is well established at potentials that are more negative to -1750 mV, regardless of the direction of the sweep in this domain. That is, the plot free of any hysteresis. It is also totally unaffected by the presence or absence of Pb^{2+} ions in solution in this domain.

Figure 3 shows the results obtained under steady-state, galvanostatic, cathodic polarization in the Tafel region for a smooth pure-lead electrode in H_2SO_4 of different concentrations in the range of 3.67 to 10.09 M. The Tafel lines are well defined with essentially the same slope over the entire concentration range. The actual location of the Tafel lines shifts towards less cathodic values as the concentration of H_2SO_4 is increased. However, the corrosion potential is unchanged at -968 ± 2 mV for all the curves.

Tafel plots for a smooth pure-lead electrode in H_2SO_4 (5.298 M) containing different amounts of H_3PO_4 additive are presented in Fig. 4. Significant features of the curves are:

(i) The H_3PO_4 additive increases the hydrogen overpotential at any given current density.

(ii) The increase in hydrogen overpotential shows a maximum at a H_3PO_4 concentration of around 20 g l^{-1}.

(iii) The slope of the Tafel plots, as well as the corrosion potential, remains the same both in the presence and the absence of H_3PO_4.

The above significant findings, are in fact, of a general nature will respect to H_2SO_4 concentration.
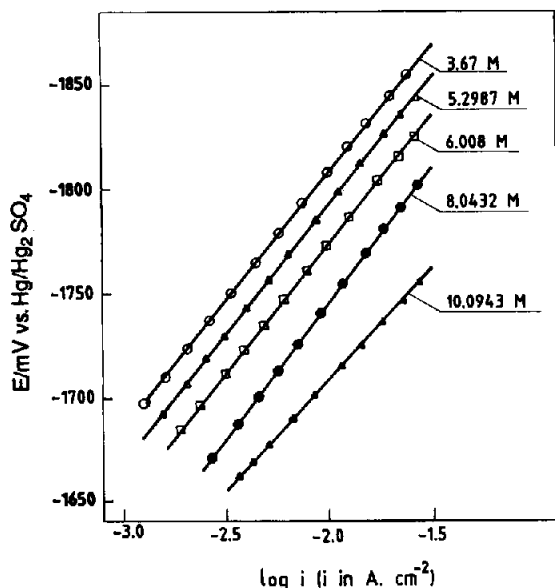

Fig. 3. Dependence of Tafel plots for HER on lead electrode on the molarity of H_2SO_4 solution (shown as inset); $E_{cor} = -968 \pm 2$ mV vs. Hg/Hg_2SO_4 for all the curves.
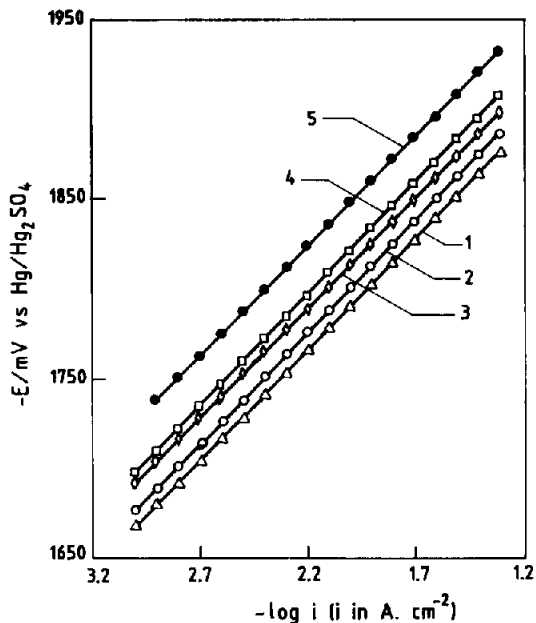
Fig. 4. Tafel plots for HER on smooth, pure-lead electrode in H_2SO_4 (5.298 M) with different concentrations of H_3PO_4, g l^{-1}: (1) 0; (2) 40; (3) 30; (4) 10, and (5) 20 g l^{-1}; $E_{cor} = -968 \pm 2$ mV vs. Hg/Hg_2SO_4 for all the curves.

Since the behaviour of H_3PO_4 additive is to be considered conjointly with its operation in a sealed lead/acid cell with a low-antimonial positive grid, it is desirable to know the influence of H_3PO_4 additive on the deleterious effect of Sb(III). These antimony ions, on migrating from the positive electrode, deposit on the negative electrode and, thereby, lowering the overpotential for the HER on the negative electrode [33].

Figure 5 shows the effect of dissolved antimony on the cathodic HER in the Tafel region on smooth pure lead in contact with 6.008 M H_2SO_4 that contains different amounts of H_3PO_4 additive. The following conclusions may be drawn from the data:

(i) The well-known decrease in the hydrogen overpotential due to dissolved antimony is demonstrated.

(ii) The H_3PO_4 additive suppresses to a large extent the adverse effect of dissolved antimony on the overpotential for the HER. In other words, the decrease in overpotential caused by a given concentration of antimony in solution is annulled considerably if H_3PO_4 additive is present in solution.

(iii) The effect of H_3PO_4 of partially off-setting the adverse influence of dissolved Sb(III) is optimal at a H_3PO_4 concentration of ~ 20 g l^{-1}.

For sealed lead/acid batteries, it is highly desirable to use a low-antimonial lead alloy grid for the positive electrode and lead–calcium or other antimony-free grid for the negative electrode. It is therefore of particular relevance to know the Tafel plot characteristics of the HER for these alloys, as well as the effect of H_3PO_4 additive with and without dissolved Sb(III) in solution. Extensive experimental investigations were therefore performed on these alloys, in a similar manner to those discussed above for smooth pure lead.
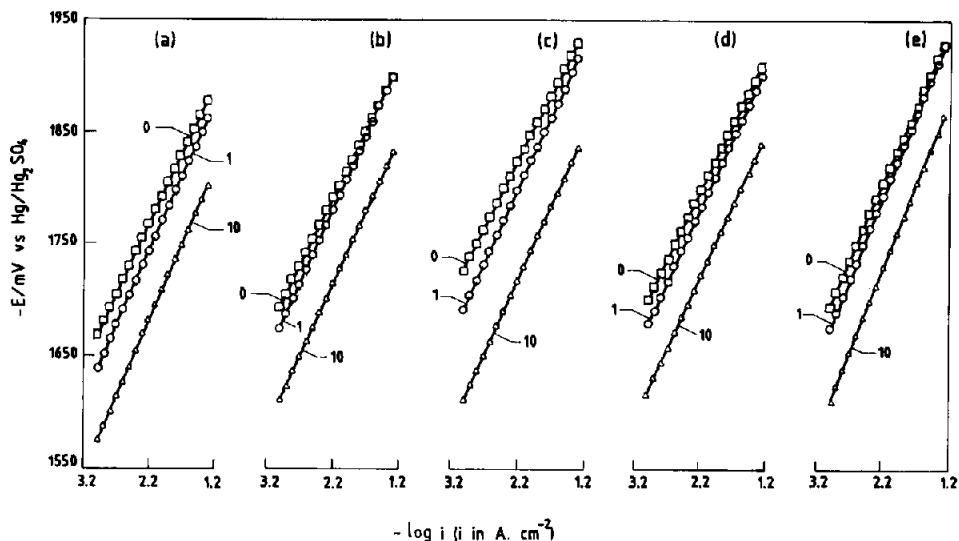
Fig. 5. Tafel plots for HER on smooth, pure-lead grid in H_2SO_4 (5.298 M) with different concentrations of H_3PO_4, g l^{-1}: (a) 0; (b) 10; (c) 20; (d) 30, and (e) 40 g l^{-1} and Sb(III), mg l^{-1} in the electrolyte (shown as inset); $E_{cor} = -968 \pm 2$ mV vs. Hg/Hg_2SO_4 for the case [Sb(III)] = 0, and -965 ± 3 mV vs. Hg/Hg_2SO_4 for the cases [Sb(III)] = 1–10 mg l^{-1}.

Typical experimental results for a Pb–Ca–Sn alloy grid electrode in contact with 6.008 M H_2SO_4 solution with H_3PO_4 additive, and in the presence or absence of antimony in solution, are presented in Fig. 6. The experimental observations may be summarised as follows:

(i) At any given concentration of sulfuric acid, H_3PO_4 additive increases the overpotential for the HER.

(ii) This increase in hydrogen overpotential is a maximum at a H_3PO_4 concentration of 20 g l^{-1}.

(iii) The decrease in hydrogen overpotential caused by dissolved Sb(III) (0 to 10 mg l^{-1}) in solution is annulled significantly by H_3PO_4 additive. The effect is a maximum at about 20 g l^{-1} of H_3PO_4.

(iv) The Tafel slopes for the HER remain unchanged and lie in the range 125 ± 5 mV in all cases where Sb(III) is absent in solution. On the other hand, when Sb(III) (1 to 10 mg l^{-1}) is present in solution, the Tafel slope for the HER is little higher (130 ± 5 mV) and shows slightly more scatter.

(v) Further, the corrosion potentials (not shown in Figs.) are unchanged at about -968 ± 2 mV in all cases where Sb(III) is absent in solution. The corrosion potentials are in the range -965 ± 3 mV in the presence of Sb(III) (1 to 10 mg l^{-1}).

The basic principle in determining the rate of electrochemical corrosion is to back extrapolate the steady-state, hysteresis-free Tafel line for the cathodic reaction (i.e., HER in acid media) up to the corrosion potential. The current at the intersection is the corrosion current under the given conditions.

From the experimental Tafel plots for the HER on pure lead and Pb–Ca–Sn electrodes in H_2SO_4 solution (3.67 to 10 M) with H_3PO_4 (0 to 40 g l^{-1}) and Sb(III) (0 to 10 mg l^{-1}) additives, the corrosion current densities were calculated by back extrapolation of the Tafel plot to the corresponding steady-state corrosion potential
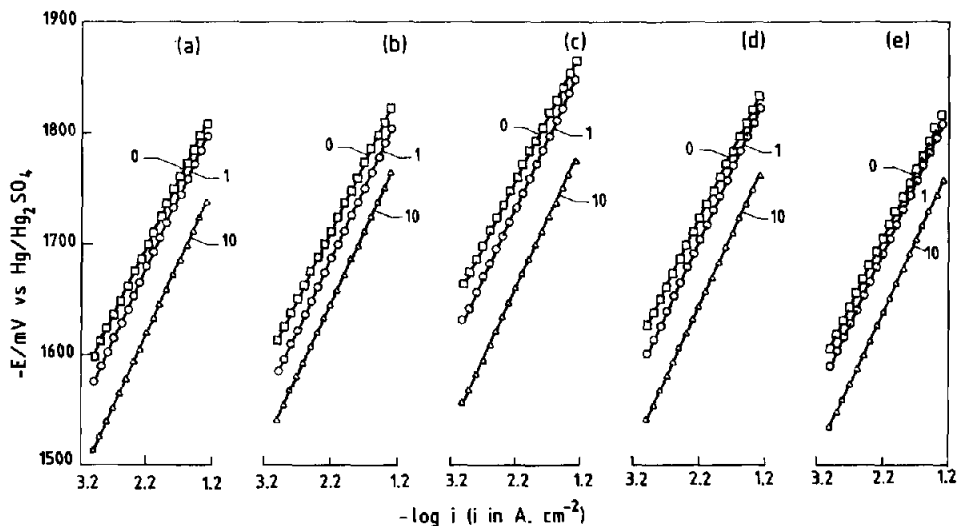
Fig. 6. Tafel plots for HER on smooth Pb–Ca–Sn alloy in H_2SO_4 (6.008 M) with different concentrations of H_3PO_4, g l^{-1}: (a) 0; (b) 10; (c) 20; (d) 30 and (e) 40 g l^{-1} and Sb(III), mg l^{-1} in the electrolyte (shown as inset); $E_{cor} = -968 \pm 2$ mV vs. Hg/Hg_2SO_4 for the case [Sb(III)] = 0, and -965 ± 3 mV vs Hg/Hg_2SO_4 for the cases [Sb(III)] = 1–10 mg l^{-1}.

(-968 ± 2 mV for Sb(III) = 0 and -965 ± 3 mV for Sb(III) = 1 to 10 mg l^{-1}). The corrosion current densities thus obtained are listed in Tables 1 to 4. The notable features that may be deduced from these data are as follows:

(i) The corrosion rate for pure lead, Pb–Ca–Sn and Pb–Sb–Se alloys increases with increasing concentration of H_2SO_4.

(ii) H_3PO_4 additive decreases the corrosion rate in all cases.

(iii) The decrease in the corrosion rate caused by the H_3PO_4 additive is largest for a 20 g l^{-1} concentration of H_3PO_4 in solution.

(iv) In the presence of dissolved Sb(III) in solution, the corrosion rate is enhanced in all cases.

(v) The enhanced corrosion rate due to dissolved antimony is diminished in the presence of H_3PO_4 as compared with the rate in the absence of this additive.

(vi) The Sb(III)-induced corrosion rate is suppressed to a large extent at a concentration of 20 g l^{-1} H_3PO_4 in solution.

The most significant observation is that H_3PO_4 suppresses the Sb(III)-induced corrosion of lead and lead alloys. This may be understood in the following way. The standard potential for the SbO^+/Sb reaction ($E^0 = +0.21$ V) is more positive than that of the $Pb/PbSO_4$ reaction ($E^0 = -0.356$ V). Therefore, the deposition of elemental antimony on the lead surface is thermodynamically feasible and is likely to occur in H_2SO_4 solution. From a kinetics point of view, this reaction of galvanic deposition of antimony on a lead surface has been proved to occur under open-circuit conditions [1, 34–36].

Since the corrosion of lead in de-aerated sulfuric acid involves only hydrogen depolarization, the rate of which is directly related to the kinetics of the HER on lead, it may be visualised that, in the presence of Sb(III) in solution, the HER will occur not only on lead but also on antimony deposited on the lead surface. The overall rate of the HER, and hence the corrosion rate of lead, are determined by the kinetics

TABLE 1

Tafel slopes and corrosion current densities for the hydrogen evolution reaction on smooth lead and Pb–Ca–Sn electrodes with phosphoric acid and Sb(III) additives to the electrolyte

Electrolyte composition	Pure Pb		Pb–Ca–Sn	
	Slope (mV per decade)	i_{cor} (A cm^{-2})	Slope (mV per decade)	i_{cor} (A cm^{-2})
H$_2$SO$_4$ (5.298 M)	122.8	1.97×10^{-9}	122.3	3.80×10^{-9}
H$_2$SO$_4$ (5.298 M) + H$_3$PO$_4$ (10 g l^{-1})	121.1	1.02×10^{-9}	122.0	3.51×10^{-9}
H$_2$SO$_4$ (5.298 M) + H$_3$PO$_4$ (20 g l^{-1})	121.6	0.575×10^{-9}	120.2	1.73×10^{-9}
H$_2$SO$_4$ (5.298 M) + H$_3$PO$_4$ (30 g l^{-1})	124.1	1.31×10^{-9}		
H$_2$SO$_4$ (5.298 M) + H$_3$PO$_4$ (40 g l^{-1})	123.5	1.81×10^{-9}	120.9	2.74×10^{-9}
H$_2$SO$_4$ (5.298 M) + [Sb(III)] (1 mg l^{-1})	131.0	7.01×10^{-9}	128.0	10.4×10^{-9}
H$_2$SO$_4$ (5.298 M) + H$_3$PO$_4$ (10 g l^{-1}) + [Sb(III)] (1 mg l^{-1})	130.9	3.65×10^{-9}		
H$_2$SO$_4$ (5.298 M) + H$_3$PO$_4$ (20 g l^{-1}) + [Sb(III)] (1 mg l^{-1})	132.8	3.26×10^{-9}	128.0	5.28×10^{-9}
H$_2$SO$_4$ (6.008 M) + H$_3$PO$_4$ (30 g l^{-1}) + [Sb(III)] (1 mg l^{-1})	132.1	3.55×10^{-9}		
H$_2$SO$_4$ (6.008 M) + H$_3$PO$_4$ (40 g l^{-1}) + [Sb(III)] (1 mg l^{-1})	133.1	4.00×10^{-9}	128.0	6.76×10^{-9}
H$_2$SO$_4$ (6.008 M) + [Sb(III)] (10 mg l^{-1})	134.2	28.7×10^{-9}	135.0	47.7×10^{-9}
H$_2$SO$_4$ (6.008 M) + H$_3$PO$_4$ (20 g l^{-1}) + [Sb(III)] (10 mg l^{-1})	133.1	13.7×10^{-9}	130.6	20.4×10^{-9}
H$_2$SO$_4$ (6.008 M) + H$_3$PO$_4$ (30 g l^{-1}) + [Sb(III)] (10 mg l^{-1})	130.9	10.3×10^{-9}		
H$_2$SO$_4$ (6.008 M) + H$_3$PO$_4$ (40 g l^{-1}) + [Sb(III)] (10 mg l^{-1})	134.0	16.9×10^{-9}	131.0	26.1×10^{-9}

TABLE 2

Tafel slopes and corrosion current densities for the hydrogen evolution reaction on smooth lead and Pb–Ca–Sn electrodes with phosphoric acid and Sb(III) additives to the electrolyte

Electrolyte composition	Pure Pb		Pb–Ca–Sn	
	Slope (mV per decade)	i_{cor} (A cm^{-2})	Slope (mV per decade)	i_{cor} (A cm^{-2})
H$_2$SO$_4$ (6.008 M)	123.6	3.07×10^{-9}	122.0	4.48×10^{-9}
H$_2$SO$_4$ (6.008 M) + H$_3$PO$_4$ (10 g l^{-1})	124.0	2.48×10^{-9}	121.0	2.29×10^{-9}
H$_2$SO$_4$ (6.008 M) + H$_3$PO$_4$ (20 g l^{-1})	120.6	6.02×10^{-9}		
H$_2$SO$_4$ (6.008 M) + H$_3$PO$_4$ (30 g l^{-1})	122.8	1.67×10^{-9}		
H$_2$SO$_4$ (6.008 M) + H$_3$PO$_4$ (40 g l^{-1})	124.7	2.92×10^{-9}	124.0	4.93×10^{-9}
H$_2$SO$_4$ (6.008 M) + [Sb(III)] (1 mg l^{-1})	131.0	9.01×10^{-9}	130.1	13.8×10^{-9}
H$_2$SO$_4$ (6.008 M) + H$_3$PO$_4$ (10 g l^{-1}) + [Sb(III)] (1 mg l^{-1})	130.0	7.02×10^{-9}		
H$_2$SO$_4$ (6.008 M) + H$_3$PO$_4$ (20 g l^{-1}) + [Sb(III)] (1 mg l^{-1})	130.8	3.11×10^{-9}	129.6	8.12×10^{-9}
H$_2$SO$_4$ (6.008 M) + H$_3$PO$_4$ (30 g l^{-1}) + [Sb(III)] (1 mg l^{-1})	131.8	6.1×10^{-9}		
H$_2$SO$_4$ (6.008 M) + H$_3$PO$_4$ (40 g l^{-1}) + [Sb(III)] (1 mg l^{-1})	130.0	6.14×10^{-9}	129.8	11.4×10^{-9}
H$_2$SO$_4$ (6.008 M) + [Sb(III)] (10 mg l^{-1})	134.0	34.2×10^{-9}	133.2	55.1×10^{-9}
H$_2$SO$_4$ (6.008 M) + H$_3$PO$_4$ (20 g l^{-1}) + [Sb(III)] (10 mg l^{-1})	132.5	13.6×10^{-9}	131.7	23.6×10^{-9}
H$_2$SO$_4$ (6.008 M) + H$_3$PO$_4$ (30 g l^{-1}) + [Sb(III)] (10 mg l^{-1})	132.0	17.3×10^{-9}		
H$_2$SO$_4$ (6.008 M) + H$_3$PO$_4$ (40 g l^{-1}) + [Sb(III)] (10 mg l^{-1})	133.0	21.6×10^{-9}	131.0	30.9×10^{-9}

TABLE 3

Tafel slopes and corrosion current densities for the hydrogen evolution reaction on smooth lead and Pb–Ca–Sn electrodes with phosphoric acid and Sb(III) additives to the electrolyte

Electrolyte composition	Pure Pb		Pb–Ca–Sn	
	Slope (mV per decade)	i_{cor} (A cm^{-2})	Slope (mV per decade).	i_{cor} (A cm^{-2})
H_2SO_4 (8.043 M)	121.0	3.39×10^{-9}	122.3	5.15×10^{-9}
H_2SO_4 (8.043 M) + H_3PO_4 (10 g l^{-1})	121.3	2.82×10^{-9}	123.0	4.07×10^{-9}
H_2SO_4 (8.043 M) + H_3PO_4 (20 g l^{-1})	120.7	1.08×10^{-9}	122.1	2.86×10^{-9}
H_2SO_4 (8.043 M) + H_3PO_4 (30 g l^{-1})	123.4	2.65×10^{-9}	122.0	3.61×10^{-9}
H_2SO_4 (8.043 M) + H_3PO_4 (40 g l^{-1})	123.7	3.98×10^{-9}	125.8	6.35×10^{-9}
H_2SO_4 (8.043 M) + [Sb(III)] (1 mg l^{-1})	131.0	12.2×10^{-9}	133.0	19.9×10^{-9}
H_2SO_4 (8.043 M) + H_3PO_4 (20 g l^{-1}) + [Sb(III)] (1 mg l^{-1})	129.0	3.52×10^{-9}	131.0	10.8×10^{-9}
H_2SO_4 (8.043 M) + H_3PO_4 (40 g l^{-1}) + [Sb(III)] (1 mg l^{-1})	132.0	11.4×10^{-9}	131.0	12.8×10^{-9}
H_2SO_4 (8.043 M) + [Sb(III)] (10 mg l^{-1})	132.0	43.1×10^{-9}	135.0	64.7×10^{-9}
H_2SO_4 (8.043 M) + H_3PO_4 (20 g l^{-1}) + [Sb(III)] (10 mg l^{-1})	130.0	15.7×10^{-9}	134.0	26.8×10^{-9}
H_2SO_4 (8.043 M) + H_3PO_4 (40 g l^{-1}) + [Sb(III)] (10 mg l^{-1})	132.0	22.5×10^{-9}	132.0	40.0×10^{-9}
H_2SO_4 (10.09 M)	120.9	7.07×10^{-9}	121.0	7.66×10^{-9}
H_2SO_4 (10.09 M) + H_3PO_4 (10 g l^{-1})	121.0	5.65×10^{-9}	121.0	4.95×10^{-9}
H_2SO_4 (10.09 M) + H_3PO_4 (20 g l^{-1})	119.5	2.05×10^{-9}	122.0	3.97×10^{-9}
H_2SO_4 (10.09 M) + H_3PO_4 (30 g l^{-1})	119.4	3.53×10^{-9}	121.0	3.86×10^{-9}
H_2SO_4 (10.09 M) + H_3PO_4 (40 g l^{-1})	120.3	5.84×10^{-9}	122.0	4.70×10^{-9}

TABLE 4

Tafel slopes and corrosion current densities for the hydrogen evolution reaction on smooth lead and Pb–Ca–Sn electrodes with phosphoric acid and Sb(III) additives to the electrolyte

| Electrolyte composition	Pure Pb		Pb–Ca–Sn	
	Slope (mV per decade)	i_{cor} (A cm^{-2})	Slope (mV per decade)	i_{cor} (A cm^{-2})
H$_2$SO$_4$ (10.09 M) + [Sb(III)] (1 mg l^{-1})	132.0	29.2×10^{-9}	131.7	29.9×10^{-9}
H$_2$SO$_4$ (10.09 M) + H$_3$PO$_4$ (10 g l^{-1}) + [Sb(III)] (10 mg l^{-1})			129.2	15.5×10^{-9}
H$_2$SO$_4$ (10.09 M) + H$_3$PO$_4$ (20 g l^{-1}) + [Sb(III)] (1 mg l^{-1})	128.0	7.43×10^{-9}	128.0	12.5×10^{-9}
H$_2$SO$_4$ (10.09 M) + H$_3$PO$_4$ (40 g l^{-1}) + [Sb(III)] (1 mg l^{-1})	129.0	17.5×10^{-9}	128.0	11.5×10^{-9}
H$_2$SO$_4$ (10.09 M) + [Sb(III)] (10 mg l^{-1})	134.0	72.8×10^{-9}	130.4	89.5×10^{-9}
H$_2$SO$_4$ (10.09 M) + H$_3$PO$_4$ (20 g l^{-1}) + [Sb(III)] (10 mg l^{-1})	130.0	33.1×10^{-9}	133.7	77.6×10^{-9}
H$_2$SO$_4$ (10.09 M) + H$_3$PO$_4$ (30 g l^{-1}) + [Sb(III)] (10 mg l^{-1})	132.0	45.2×10^{-9}	132	50.2×10^{-9}
H$_2$SO$_4$ (10.09 M) + H$_3$PO$_4$ (40 g l^{-1}) + [Sb(III)] (10 mg l^{-1})	122.3	1.39×10^{-9}	131.4	50.9×10^{-9}
H$_2$SO$_4$ (3.67 M)	122.0	1.13×10^{-9}		
H$_2$SO$_4$ (3.67 M) + H$_3$PO$_4$ (10 g l^{-1})	120.2	0.807×10^{-9}		
H$_2$SO$_4$ (3.67 M) + H$_3$PO$_4$ (20 g l^{-1})	120.6	0.923×10^{-9}		
H$_2$SO$_4$ (3.67 M) + H$_3$PO$_4$ (30 g l^{-1})	123.8	1.50×10^{-9}		
H$_2$SO$_4$ (3.67 M) + H$_3$PO$_4$ (40 g l^{-1})				
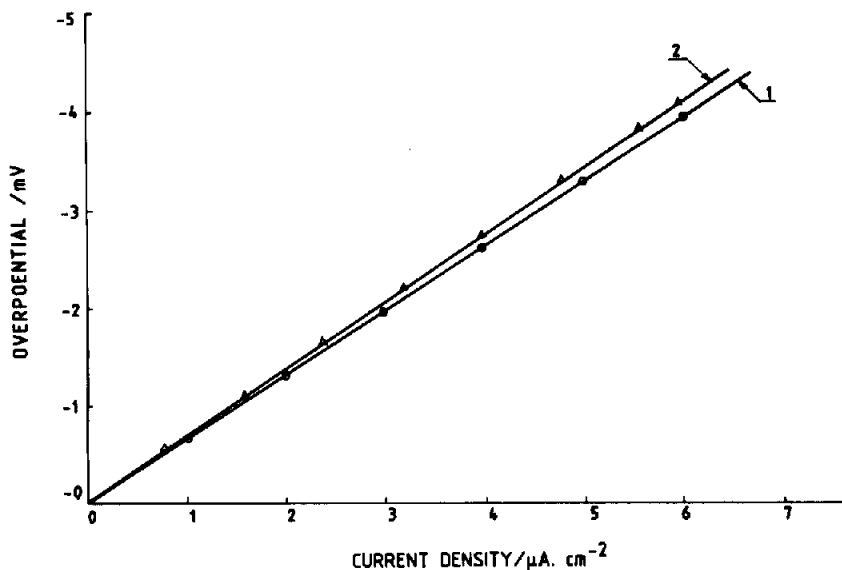
Fig. 7. Steady-state galvanostatic linear polarization for smooth lead electrode in stirred solution saturated with lead sulfate: (1) H_2SO_4 (5.298 M), and (2) H_2SO_4 (5.298 M) + H_3PO_4 (20 g l^{-1}).

of the HER on both lead and antimony. Since the overpotential for the HER on antimony is quite low [37–39] compared with that on lead, the HER will occur at a significant rate on antimony and, thereby, will increase the rate of corrosion of lead. The mechanism of suppression of this antimony-induced corrosion of lead and lead alloys by H_3PO_4 is to be attributed to a strong adsorption of H_3PO_4 on the antimony surface. Adsorption of H_3PO_4 at the interface retards the kinetics of the HER at the interface without changing the Volmer mechanism [40].

The implication of the above novel finding that H_3PO_4 suppresses the antimony-induced corrosion of pure lead and Pb–Ca–Sn alloy is of considerable importance to the design of sealed lead/acid batteries. It must be established, however, that the H_3PO_4 additive does not affect adversely the kinetics of the desired Pb/Pb^{2+} reaction at the negative electrode.

In order to determine the influence, if any, of H_3PO_4 on the kinetics of the Pb/$PbSO_4$ reaction at the negative electrode, steady-state, galvanostatic, cathodic polarization experiments in the low-overpotential region were made on a smooth, pure-lead electrode in hydrogen saturated, $PbSO_4$ saturated, well-stirred sulfuric acid, with and without H_3PO_4 additive. Saturation of the electrolyte solution with $PbSO_4$ was necessary in order to ensure that Pb^{2+} discharge occurs without any mass-transfer polarization, at least in the low overpotential domain. The results are presented in Fig. 7. There is a very good linearity through the origin for both the curves up to at least 4 mV of polarization. Further, the two straight lines almost merge with each other and this suggests that the kinetics of the electrode reaction (Pb/$PbSO_4$ reaction in this case) is the same in both cases.

Conclusions

Benefits are to be gained from the presence of H_3PO_4 at about 20 g l^{-1} in the H_2SO_4 electrolyte used in sealed lead/acid batteries. The additive has no adverse

influence on the desired reaction, but hinders the unwanted HER both in the presence and in the absence of Sb(III) in the electrolyte. These new findings, when combined with the other known advantageous effects of this additive on the performance of the positive electrode, suggest the possibility that H_3PO_4 additive to the electrolyte of sealed lead/acid batteries will minimize the present limitations and improve significantly the performance of such batteries.

Acknowledgements

References

1 A.A. Jenkins, W.C. Maskell and F.L. Tye, *J. Power Sources, 19* (1987) 75–80.
2 A.F. Hollenkamp, *J. Power Sources, 36* (1991) 567–585.
3 D. Berndt and H. Franke, *Proc. Int. Telecommunication Energy Conf., Stockholm, Sweden,* 1987, p. 115.
4 J. Szymborski and M.L. Eggerrs, *Proc. Int. Telecommunication Energy Conf.,* Institute of Electric and Electronic Engineers, Piscatoway, NJ, USA, 1982, p. 410.
5 H. Doring, K. Wiesener, J. Garche and W. Fischer, *J. Power Sources, 38* (1992) 261–272.
6 S. Masaaki, K. Takahashi, *Jpn. Patent No. 04 32 164* (Feb. 4, 1992).
7 E. Voss, *J. Power Sources, 24* (1988) 171.
8 R. Janakiraman, P.G. Balakrishnan, M. Devasahayam and S. Palanichamy, *Electrochemistry, 4* (1988) 563–564.
9 W. Visscher, *J. Power Sources, 1* (1976/77) 257–266.
10 J. Garche, H. Doring and K. Wiesener, *J. Power Sources, 33* (1991) 213.
11 O. Ikeda, C. Iwakura, H. Yoneyama and H. Tamura, *Technol. Rep. Osaka Univ., 36* (1986) 397–403.
12 K.R. Bullock and D.H. McClelland, *J. Electrochem. Soc., 123* (1976) 327.
13 P. Ruetschi and R.T. Angstadt, *J. Electrochem. Soc., 105* (1958) 555.
14 O.Z. Rasina, A.I. Aguf and M.A. Dasoyan, *Z. Prikl. Khim., 58* (1985) 1039.
15 S. Tudor, A. Wisstuch and S.H. Davang, *Electrochem. Technol., 3* (1965) 90; *4* (1966) 406; *5* (1967) 21.
16 U. Hullmeine, E. Voss and A. Winsel, *J. Power Sources, 30* (1990) 99–105.
17 K.R. Bullock and D.H. McClelland, *J. Electrochem. Soc., 124* (1977) 1478.
18 K.R. Bullock, *J. Electrochem. Soc., 126* (1979) 360; *126* (1979) 1848.
19 S. Sternberg, V. Branzoi and L. Apateanu, *J. Power Sources, 30* (1990) 177.
20 G.A. Morris, P.J. Mitchell, N.A. Hampson and J.I. Dyson, in T. Keily and B.W. Baxter (eds.), *Power Sources 12,* Int. Power Sources Symp. Committtee, Leatherhead, UK, 1989, pp. 61–75.
21 S. Sternberg, A. Mateescu, V. Branzoi and L. Apateanu, *Electrochim. Acta, 32* (1987) 349–354.
22 J.S. Enochs, R.M. Meighan, C.W. Fleischmann and D.P. Boden, *Intersoc. Energy Conv. Eng. Conf., San Francisco, CA, USA, 1984,* pp. 850–856.
23 ILZRO Annual Report, *Combined Research Projects LE-82 and LE-84,* No. 2 (1967).
24 Y. Song, J. Chen, *Dianchi, 21* (1991) 9.
25 A.A. Jenkins and W.C. Maskell, *Analyst (London), 110* (1985) 1431.
26 M.I. Gillibrand and G.R. Lomax, *Trans. Faraday Soc., 55* (1959) 643.

27 K. Vijayamohanan, S. Sathyanarayana and S.N. Joshi, *J. Power Sources, 30* (1990) 169–175.
28 K. Murugan, P.G. Balakrishnan and P.V. Vasudeva Rao, *J. Power Sources, 34* (1991) 289–301.
29 J.M. Kolotyrkin, *Proc. Int. Committee Electrochemical Thermodynamics and Kinetics, 9th Meet.*, Butterworths, London, 1959, pp. 406–419.
30 M. Hayes and A.T. Kuhn, in A.T. Kuhn (ed.), *The Electrochemistry of Lead*, Academic Press, London, 1979, 201–203.
31 P. Delahay (ed.), *Double Layer and Electrode Kinetics*, Wiley–Interscience, New York, 1965.
32 A.N. Frumkin, in P. Delahay and C.W. Tobias (eds.), *Advances in Electrochemistry and Electrochemical Engineering*, Vol. 3, Wiley–Interscience, 1963, p. 296.
33 T. Laitinen, K. Salmi, G. Sundholm, B. Monahov and D. Pavlov, *Electrochim. Acta, 36* (1991) 605–614.
34 J.L. Dawson, M.I. Gillibrand and J. Wilkinson, in D.H. Collins (ed.), *Power Sources 3*, Oriel Press, Newcastle upon Tyne, 1971, p. 1.
35 F. Burbank, A.C. Simon, E. Willihnganz, in P. Delahay and C.W. Tobias (eds.), *Advances in Electrochemistry and Electrochemical Engineering*, Vol. 8, Wiley–Interscience, New York, 1970, p. 229–245.
36 H. Bode, *Lead–Acid Batteries*, Wiley–Interscience, New York, 1977, pp. 238–242.
37 I.A. Aguf and M.A. Dasoyan, *Sov. J. Appl. Chem., 32* (1959) 2022.
38 M. Barak, *Electrochemical Power Sources*, Peter Peregrinus Ltd., Stevenage, 1980, p. 200.
39 P. Ruetschi and R.T. Angstadt, *J. Electrochem. Soc., 105* (1958) 555.
40 J.O'M. Bockris and A.K.N. Reddy, *Modern Electrochemistry*, Vol. 2, Plenum, New York, 1970, p. 1250.